1521-0111/12/8204-687–699$25.00
MOLECULAR PHARMACOLOGY
Copyright © 2012 The American Society for Pharmacology and Experimental Therapeutics
Mol Pharmacol 82:687–699, 2012

Vol. 82, No. 4
80291/3795142

Synthesis of Selective Agonists for the α7 Nicotinic Acetylcholine Receptor with In Situ Click-Chemistry on Acetylcholine-Binding Protein Templates[S]

John G. Yamauchi, Kimberly Gomez, Neil Grimster, Mikael Dufouil,[1] Ákos Nemecz, Joseph R. Fotsing,[2] Kwok-Yiu Ho, Todd T. Talley,[3] K. Barry Sharpless, Valery V. Fokin, and Palmer Taylor

Department of Pharmacology, Skaggs School of Pharmacy and Pharmaceutical Sciences (J.G.Y., K.G., M.D., Á.N., K.H., T.T.T., P.T.), and Department of Chemistry and Biochemistry, Division of Physical Sciences (Á.N.), University of California, San Diego, La Jolla, California; and Skaggs Institute for Chemical Biology, Scripps Research Institute, La Jolla, California (N.G., M.D., J.R.F., K.B.S., V.V.F.)

Received May 28, 2012; accepted July 11, 2012

ABSTRACT

The acetylcholine-binding proteins (AChBPs), which serve as structural surrogates for the extracellular domain of nicotinic acetylcholine receptors (nAChRs), were used as reaction templates for in situ click-chemistry reactions to generate a congeneric series of triazoles from azide and alkyne building blocks. The catalysis of in situ azide-alkyne cycloaddition reactions at a dynamic subunit interface facilitated the synthesis of potentially selective compounds for nAChRs. We investigated compound sets generated in situ with soluble AChBP templates through pharmacological characterization with α7 and $\alpha4\beta2$ nAChRs and 5-hydroxytryptamine type 3A receptors. Analysis of activity differences between the triazole 1,5-*syn*- and 1,4-*anti*-isomers showed a preference for the 1,4-*anti*-triazole regioisomers among nAChRs. To improve nAChR subtype selectivity, the highest-potency building block for α7 nAChRs, i.e., 3α-azido-*N*-methylammonium tropane, was used for additional in situ reactions with a mutated *Aplysia californica* AChBP that was made to resemble the ligand-binding domain of the α7 nAChR. Fourteen of 50 possible triazole products were identified, and their corresponding tertiary analogs were synthesized. Pharmacological assays revealed that the mutated binding protein template provided enhanced selectivity of ligands through in situ reactions. Discrete trends in pharmacological profiles were evident, with most compounds emerging as α7 nAChR agonists and $\alpha4\beta2$ nAChR antagonists. Triazoles bearing quaternary tropanes and aromatic groups were most potent for α7 nAChRs. Pharmacological characterization of the in situ reaction products established that click-chemistry synthesis with surrogate receptor templates offered novel extensions of fragment-based drug design that were applicable to multisubunit ion channels.

Introduction

Cys-loop receptors are pentameric, ligand-gated, ion channels (pLGICs) that are defined by two extracellular, disulfide-linked cysteine residues. Other family members include the 5-HT_3, $GABA_A$, $GABA_C$, glycine, and invertebrate glutamate and histamine receptors (Karlin, 2002). The nAChRs are activated by the excitatory neurotransmitter acetylcholine and are located at synapses in the CNS, neuromuscular junctions, and peripheral autonomic ganglia. They are widely distributed in the brain and mediate functions such as motor and autonomic activity, memory, and cognitive perceptions.

This work was supported by the National Institutes of Health National Institute of General Medical Sciences [Grants T32-GM07752, R01-GM18360-39, R01-GM087620]; the National Institutes of Health National Institute on Drug Abuse [Grant U01-DA019372]; and the National Science Foundation [Grant GK-12 0742551].

[1] Current affiliation: University Claude Bernard Lyon 1, Villeurbanne, France.

[2] Current affiliation: Senomyx, San Diego, California.

[3] Current affiliation: Department of Biomedical and Pharmaceutical Sciences, College of Pharmacy, Idaho State University, Pocatello, Idaho.

Article, publication date, and citation information can be found at http://molpharm.aspetjournals.org.

http://dx.doi.org/10.1124/mol.112.080291.

[S] The online version of this article (available at http://molpharm.aspetjournals.org) contains supplemental material.

ABBREVIATIONS: pLGIC, pentameric, ligand-gated ion channel; 5-HT, 5-hydroxytrypamine; AChBP, acetylcholine-binding protein; MT2, mutant 2; CNiFER, cell-based neurotransmitter fluorescently engineered reporter; CNS, central nervous system; CuAAC, copper-catalyzed azide-alkyne cycloaddition; DR, dose ratio; MLA, methyllycaconitine; nAChR, nicotinic acetylcholine receptor; TFA, trifluoroacetic acid; PDB, Protein Data Bank; HEK, human embryonic kidney; MS, mass spectrometry; LC, liquid chromatography; PNU-120596, *N*-(5-chloro-2,4-dimethoxyphenyl)-*N′*-(5-methyl-3-isoxazolyl)urea.

The $\alpha7$ and $\alpha4\beta2$ nAChRs on pyramidal neurons and interneurons of the hippocampus contribute to synaptic plasticity, memory, and learning by regulating the release of excitatory (glutamate) and inhibitory (GABA) neurotransmitters (Kenney and Gould, 2008). Because of extensive associations with cholinergic neurotransmission in neurodegenerative and developmental diseases, nAChRs have been considered pharmaceutical targets for CNS disorders (Mudo et al., 2007; Kenney and Gould, 2008; Picciotto and Zoli, 2008). The two most abundant subtypes in the brain, i.e., $\alpha7$ and $\alpha4\beta2$ nAChRs, have been targeted for the development of selective orthosteric and allosteric therapeutic ligands for the treatment of Alzheimer's disease, schizophrenia, and Parkinson's disease and the promotion of smoking cessation (Taly et al., 2009). Obtaining subtype-selective ligands for nAChRs has been challenging, because of the multiplicity of receptor subtypes and their discrete CNS locations (Millar and Gotti, 2009).

The azide-alkyne click-chemistry approach involves highly exergonic, biorthogonal, cycloaddition reactions that yield five-membered 1,2,3-triazoles in either the 1,4-*anti*- or 1,5-*syn*-isomer conformation (Scheme 1). The triazole moiety formed is stable and is largely resistant to degradation and metabolism (Kolb and Sharpless, 2003). The basicity of the N2 and N3 atoms of 1,2,3-triazoles is sufficiently low (pK_a values of the conjugate acids of 1.5–2.0) that they remain uncharged at physiological pH values. However, the triazole ring exhibits a relatively strong dipole moment of ~5 debyes (Purcell and Singer, 1967), and the N2 and N3 atoms serve as weak hydrogen-bond acceptors. Triazoles formed in cycloaddition reactions may be regarded as small spacer rings, in which intersite distances can be controlled by the regioisomer formed through linear linkers between the azide and alkyne moieties.

The freeze-frame click-chemistry approach, with a flexible target template, has the advantage of the reactant building blocks selecting a conformation preferred by the reaction product, which yields a conformation specific to the bound ligand state. Contemporary drug discovery has encompassed fragment-based drug design; moreover, in situ, freeze-frame, click-chemistry methods allow the target of drug action to serve as the template. Earlier successful applications that generated lead compounds through in situ click-chemistry methods involved enzyme templates, including acetylcholinesterase (Lewis et al., 2002), carbonic anhydrase (Mocharla et al., 2004), and HIV protease (Whiting et al., 2006). The enzyme templates contained sequestered, often deep, active-site pockets to stabilize the association of azide and alkyne building blocks and to facilitate the cycloaddition reaction.

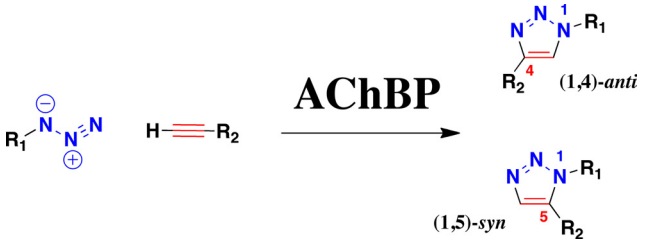

Scheme 1. Generation of 1,4-*anti*- and 1,5-*syn*-1,2,3-triazoles with AChBP templates. Reactions performed with biological templates such as the AChBPs to synthesize compounds in situ can potentially produce 1,4-*anti*- and 1,5-*syn*-triazole products, but separation of the two types with LC/MS was not possible.

We were interested in expanding the in situ click-chemistry approach with templates for pharmacologically relevant neurotransmitter receptors, such as the nAChR and its Cys-loop cousins. However, performing these reactions with native receptors presents challenges regarding template and product isolation in membrane environments, as well as conformation of the product to an intersubunit binding site that typically exhibits cooperative interactions. By using soluble surrogates of the extracellular domain of nAChR subunits, i.e., the acetylcholine-binding proteins (AChBPs) from *Lymnaea stagnalis* (Brejc et al., 2001; Smit et al., 2001) and *Aplysia californica* (Hansen et al., 2004), we generated azide-alkyne cycloaddition products in situ at the orthosteric sites of the subunit interfaces of these oligomeric proteins, with dissociation constants extending into the low nanomolar range (Grimster et al., 2012). The azide and alkyne components forming triazoles were identified through LC/MS. Identified regioisomers were then synthesized in larger amounts by using Cu(I)-catalyzed azide-alkyne cycloaddition (CuAAC) for the *anti*-regioisomers, (Rostovtsev et al., 2002; Tornøe et al., 2002) and Ru(II)-catalyzed azide-alkyne cycloaddition for the *syn*-regioisomers, (Zhang et al., 2005; Majireck and Weinreb, 2006). Because in situ 1,2,3-triazole cycloaddition reactions potentially yield 1,4-*anti*- and 1,5-*syn*-regioisomer products, both isomers were synthesized individually in the absence of the template (Scheme 2).

Here we characterize the pharmacological selectivity of previously reported click-chemistry lead compounds generated in situ on soluble *L. stagnalis*, *A. californica*, and *A. californica* Y55W AChBPs (Grimster et al., 2012) with $\alpha7$ and $\alpha4\beta2$ nAChRs, as well as 5-HT_{3A} pLGICs (Scheme 1). Furthermore, we used a mutated *A. californica* AChBP template (Nemecz and Taylor, 2011) that showed greater sequence identity with respect to the $\alpha7$ nAChR to synthesize compounds that were more selective for the $\alpha7$ nAChR. Our extension of the in situ click-chemistry approach to the pLGIC class of membrane-bound receptors expands reaction diversity and candidate/lead applications to other targeted receptor systems.

Materials and Methods

Cell Lines and AChBP Purification. Cells were cultured in 10-cm plates with Dulbecco's modified Eagle medium (Mediatech, Manassas, VA) supplemented with 10% fetal bovine serum (Gemini Bio-Products, West Sacramento, CA) and 1% glutamine (Invitrogen, Carlsbad, CA) and were incubated at 37°C with 10% CO_2. Stable cell-based neurotransmitter fluorescently engineered reporter (CNiFER)

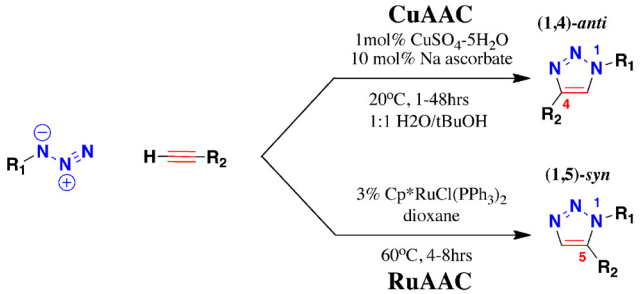

Scheme 2. Synthesis of individual 1,2,3-triazole regioisomers with metal catalysts. Experimental reactions were performed with metal catalysts to produce specific isomers of 1,2,3-triazole compounds, i.e., Cu(I) for 1,4-*anti*-isomers and Ru(II) for 1,5-*syn*-isomers.

cell lines expressing either human $\alpha7$ nAChRs with RIC3 (HEKtsA201 cells), human $\alpha4\beta2$ nAChRs (HEKtsA201 cells), or mouse 5-HT_{3A} receptors (HEK293 cells) were prepared as described previously (Yamauchi et al., 2011). Each CNiFER cell line contained the genetically encoded Ca^{2+} sensor TN-XXL (Mank et al., 2008), for measurements of Ca^{2+} flux through the pLGICs. Cells expressing $\alpha4\beta2$ nAChRs presumably contained both subtype stoichiometries, as described previously (Kuryatov et al., 2005). AChBP purification and expression of *L. stagnalis*, *A. californica*, *A. californica* Y55W, and *A. californica* MT2 AChBPs were performed as described previously (Hansen et al., 2005; Talley et al., 2006; Nemecz and Taylor, 2011). Amino-terminally FLAG-tagged AChBPs were expressed in stable HEK293S cells lacking the *N*-acetylglucosaminyl-transferase I gene (HEK293S GnTI−) (Reeves et al., 2002). AChBPs were purified with anti-FLAG antibody-conjugated resin and eluted with FLAG peptide (Sigma-Aldrich, St. Louis, MO). Pentameric assembly was assessed through size exclusion chromatography with a Superose 6 10/300 GL column (GE Healthcare, Chalfont St. Giles, Buckinghamshire, UK) with 50 mM Tris-HCl (pH 7.4), 150 mM NaCl, 0.02% sodium azide. Purified AChBP pentamers were concentrated by filtration (Amicon; Millipore Corp., Billerica, MA) to a final concentration of 5 mg/ml.

Flex Assays with CNiFER Cells. The CNiFER assay identified and characterized compounds as agonists or antagonists on the basis of peak Förster resonance energy transfer responses mediated through Ca^{2+} flux through the pLGICs (Yamauchi et al., 2011). Ninety-six-well poly-D-lysine-coated, black, clear-bottomed plates (E&K Scientific Products, Santa Clara, CA) were treated through incubation of the wells with 50 μl of 0.1 mg/ml poly-D-lysine (Sigma-Aldrich) for 30 min and then were washed with Dulbecco's phosphate-buffered saline (Mediatech). Cells were plated onto the 96-well plates 1 day before assays and were incubated at 37°C in 10% CO_2. The medium was replaced with 100 μl of artificial cerebrospinal fluid, including specified antagonists or positive allosteric modulators according to the assay, and cells were incubated at 37°C for ~30 min before responses were measured. All artificial cerebrospinal fluid buffers for assays performed with $\alpha7$ nAChRs contained 10 to 15 μM *N*-(5-chloro-2,4-dimethoxyphenyl)-*N*′-(5-methyl-3-isoxazolyl)urea (PNU-120596) (Tocris Bioscience, Ellisville, MO). A FlexStation III system (Molecular Devices, Sunnyvale, CA) was used to inject compounds and to measure fluorescence responses. Mean EC_{50} values for each agonist were calculated from at least three experiments. Varied antagonist concentrations were used to measure competitive and noncompetitive inhibition, and results were referenced to a control agonist concentration-response curve. The potencies of competitive antagonists (K_A values) were calculated by using Schild analyses (Arunlakshana and Schild, 1959; Wyllie and Chen, 2007) of dose ratios (DRs) or by using the linear relationship $K_A = [A]/(DR - 1)$, where [A] is the antagonist concentration (Taylor and Insel, 1990). The constants for noncompetitive antagonists (K_A) were defined as $IC_{50} = K_A$ and were calculated by using the equation $K_A = [A]/[(\Delta_{max}/\Delta) - 1]$, where Δ/Δ_{max} is the fraction of the maximal response. Values are reported as arithmetic means with S.D. values.

Agonist Screens. Basal fluorescence levels were recorded for 30 s, followed by the addition (50 μl/well) of test ligands prepared in buffer at 3 times (40 μM) the final concentration (13.3 μM). Measurements were made at 3.54-s intervals for each emission wavelength over 120 s, to assess the potential agonist behavior of each ligand. Control wells were used to normalize the responses of the test compounds; buffer was used to measure background fluorescence, 0.1 and 1 μM (±)-epibatidine ($\alpha7$ and $\alpha4\beta2$ nAChRs) and 1 μM 5-HT (5-HT_{3A} receptors) were used as agonist references, and 1 μM MLA ($\alpha7$ nAChRs), 10 μM dihydro-β-erythroidine ($\alpha4\beta2$ nAChRs), and 0.1 and 1 μM tropisetron (5-HT_{3A} receptors) were used as antagonist references. Agonist responses were normalized as corrected fractions through subtraction of background fluorescence values. Three or four activity screens were performed, with three replicates per screen, and overall means and S.D. values were calculated from the mean values for each screen. Compounds that produced normalized fractional agonist responses of ≥0.2 were identified as agonists and were further characterized with EC_{50} values determined from concentration-response curves.

Antagonist Screens. Directly after the agonist screens, which required approximately 25 to 35 min to complete, 50 μl of a reference agonist at the maximal response concentration (prepared at 4 times the final concentration) was injected into each well, for assessment of the potential antagonist properties of tested compounds (10 μM final concentration). Final concentrations of 0.1 or 1 μM (±)-epibatidine ($\alpha7$ and $\alpha4\beta2$ nAChRs) or 1 μM 5-HT (5-HT_{3A} receptors) were used for agonists for assessment of inhibition by the test compounds. Responses were normalized as fractions of antagonist inhibition. The numbers of screens performed and the calculation of values were as described for the agonist screens. Compounds with inhibition fractions of ≥0.5 were characterized further, to derive K_A values for competitive or noncompetitive inhibition.

Radioligand Binding Assays. The AChBP scintillation proximity assay was used to determine apparent K_d values for the compounds, as reported previously (Talley et al., 2006). AChBP (0.5–1.0 nM final concentrations at the binding site), anti-mouse Ig polyvinyltoluene scintillation proximity assay beads (0.17 mg/ml final concentration; PerkinElmer Life and Analytical Sciences, Waltham, MA), mouse monoclonal anti-FLAG M2 antibody (1:8000 dilution; Sigma-Aldrich), and (±)-[^{3}H]epibatidine (PerkinElmer Life and Analytical Sciences) were combined in 0.1 M sodium phosphate buffer (pH 7.0). Nonspecific binding was determined in parallel through the addition of a saturating concentration (12.5 μM) of MLA (Tocris Bioscience) to an identical set of wells. Competition assays were conducted with a constant concentration of (±)-[^{3}H]epibatidine (5–20 nM final concentration) for each AChBP and varying concentrations of competing ligand. At least three independent experiments, performed in duplicate, were used to determine K_d values as arithmetic means with S.D. values.

In Situ Synthesis from Azide and Alkyne Libraries. 3α-Azido-*N*-methylammonium tropane (100 mM) was dissolved in 0.1 M sodium phosphate buffer (pH 7.0). Fifty alkynes were dissolved in dimethylsulfoxide and were combined to yield a final alkyne concentration of 50 mM. The 3α-azido-*N*-methylammonium tropane solution (10 μl) was added to *A. californica* MT2 AChBP (~1 mg/ml in 0.1 M sodium phosphate buffer, pH 7.0; 980 μl) in a microfuge tube, followed immediately by the combined alkyne solution (10 μl). The reactants were briefly mixed and then incubated at room temperature. In a separate microfuge tube, 3α-azido-*N*-methylammonium tropane (100 mM in 0.1 M sodium phosphate buffer, pH 7.0; 10 μl) and the combined alkyne solution (50 mM in dimethylsulfoxide; 10 μl) were diluted with water (870 μl) before the addition of aqueous copper sulfate (0.05 M; 10 μl) and aqueous sodium ascorbate (0.1 M; 100 μl). The reactants were mixed and then incubated at room temperature.

After 10 days, both samples were analyzed, in triplicate, by using LC/MS with selected-ion monitoring with a Zorbax reverse-phase column (4.6 mm × 3 cm, SB-C18, rapid resolution; Agilent Technologies, Santa Clara, CA) preceded by a Phenomenex C18 guard column (Phenomenex, Torrance, CA); the flow rate was 0.5 ml/min, and gradient elution was performed as follows: water plus 0.05% TFA/acetonitrile plus 0.05% TFA from 100:0 to 0:100 over 15 min and then 100% acetonitrile plus 0.05% TFA for 5 min, with a post-run time of 5 min with the starting solvent ratio. MS detection was performed through electrospray ionization mass spectrometry with positive selected-ion monitoring. To increase MS detection sensitivity, 10 injections (25 μl each) were performed; each injection was tuned to detect five of the expected 50 molecular weights. The cycloaddition products of the in situ screen were identified on the basis of their molecular weights and comparisons of retention times for the formed products with the values determined in analyses of the copper-catalyzed reactions. A control experiment, performed as described above, substituted bovine serum albumin (1 mg/ml) for *A.*

californica MT2 AChBP. LC/MS with selected-ion monitoring detected no triazole products in the presence of bovine serum albumin.

Results

Compounds Generated In Situ with *L. stagnalis*, *A. californica*, and *A. californica* Y55W AChBPs. We were interested initially in investigating the functional nAChR activity of compounds (**1**-**9**) that were identified and generated previously by using azide-alkyne in situ click-chemistry methods, with *L. stagnalis*, *A. californica*, and *A. californica* Y55W AChBPs as reaction templates (Grimster et al., 2012). The 1,4-*anti*-isomers were examined initially, because they could be synthesized in larger quantities through CuAAC. We were also interested in differences between triazole regioisomers; therefore, we synthesized the triazolic 1,5-*syn*-isomers (**1′**–**5′**) of compounds **1** to **5**. The chemical structures of triazoles **1** to **5**, **1′** to **5′**, and **6** to **9** are shown in Table 1. Initial data on agonist and antagonist activities, or a lack thereof, at $\alpha7$ and $\alpha4\beta2$ nAChRs and 5-HT_{3A} receptors are shown in Supplemental Fig. 1.

Pharmacological tests with $\alpha7$ nAChRs identified all 14 triazole compounds as agonists and none as antagonists at 13.3 μM. Notably, the 1,4-*anti*-triazoles **1** and **3** exhibited slightly higher agonist activities (potencies) than did the 1,5-*syn*-isomers **1′** and **3′** (Supplemental Fig. 1A). Agonist responses elicited at $\alpha7$ nAChRs by these compounds were blocked with 1 μM MLA (Mogg et al., 2002), to establish that the responses were specific to the transfected $\alpha7$ nAChRs (Supplemental Fig. 2). The $\alpha7$ nAChR agonists were characterized with concentration-response curves, and the 1,4-*anti*-isomers showed slightly greater potencies, i.e., 2- to 3-fold greater for $\alpha7$ nAChR agonists, except in the case of **1** and **3**, and 2- to 6-fold greater for $\alpha4\beta2$ nAChR competitive antagonists, except in the case of **1** (Supplemental Table 1). This general trend held true for binding of the 1,4-*anti*- and 1,5-*syn*-triazoles to the three AChBPs (Table 1; Supplemental Table 1). Triazoles **4** and **4′** exhibited slight differences in K_d (1.0 and 2 nM) and EC_{50} (0.3 and 0.6 μM) values for *L. stagnalis* AChBP and $\alpha7$ nAChRs, respectively (both with 2-fold activity ratios), whereas substantial differences were seen for *A. californica* (24 and 300 nM) and *A. californica* Y55W (17 and 100 nM) AChBPs (with activity ratios of 13 and 5.8, respectively) (Table 1; Supplemental Table 1). Triazole **4** showed the highest overall affinity for $\alpha7$ nAChRs among the 1,4-*anti*-compounds tested (Fig. 1).

None of the 14 compounds tested at 13.3 μM was an agonist for $\alpha4\beta2$ nAChRs, whereas eight (**1**-**5**, **6**, **8**, and **9**) were found to be antagonists at 10 μM (Supplemental Fig. 1B). A Schild analysis was performed with graded responses derived from the incubation of various concentrations of the antagonists for 30 min before the addition of agonist to $\alpha4\beta2$ nAChR-expressing CNiFER cells. The well characterized $\alpha4\beta2$ nAChR antagonists dihydro-β-erythroidine and mecamylamine produced inhibition profiles with the expected competitive and noncompetitive characteristics, respectively (Fig. 2), and served as reference indicators for those types of antagonism.

Measurements of ion permeability over a period of several seconds incur distortions resulting from possible desensitization and changes in intracellular ion distribution. However, the sample throughput allows for multiple measurements of agonist responses and antagonist block with the Schild null method. This approach is particularly useful for distinguishing agonist responses from antagonist responses and rank-ordering potencies across multiple receptor subtypes.

Despite overall structural similarities, the triazole antagonists exhibited a variety of apparent mixed competitive and noncompetitive inhibition profiles. Triazole **4** was the most potent antagonist for $\alpha4\beta2$ nAChRs, with a measured competitive K_A value of 4 μM, and was 5.8-fold more potent than its 1,5-*syn*-counterpart **4′** (Table 1; Supplemental Table 1; Fig. 3). Although both compounds showed noncompetitive characteristics at concentrations above 10 μM, the competitive component was significantly stronger for **4**, as seen in the profile of the curves obtained with 3 and 10 μM (Fig. 3A). Compound **4′** showed less competitive inhibition than did **4**, with nearly equal contributions of competitive and noncompetitive inhibition (Fig. 3B). Overall, the competitive components of inhibition were stronger than the noncompetitive components with $\alpha4\beta2$ nAChRs (Supplemental Table 2). The 14 compounds tested were all weaker as antagonists with $\alpha4\beta2$ nAChRs than as agonists with $\alpha7$ nAChRs, with differences in some cases being >10-fold (Table 1; Supplemental Table 3).

None of the compounds displayed agonist activity when tested with 5-HT_{3A} receptors at 13.3 μM, and only the triazole **4′** was found to be an antagonist at 10 μM (Supplemental Fig. 1C). The inhibition profile for **4′** showed competitive blocking of 5-HT elicited responses with a calculated competitive K_A value of 0.9 μM (Fig. 4A). Its triazolic 1,4-*anti*-isomer **4** was found to be a much weaker 5-HT_{3A} receptor antagonist, with a competitive K_A value of 34 μM (Fig. 4C), which translated to a 38-fold greater potency of inhibition for the 1,5-*syn*-isomer **4′**. Compared with $\alpha7$ and $\alpha4\beta2$ nAChRs, which preferred the 1,4-*anti*-isomers, 5-HT_{3A} receptors showed a preference for the *N*-methylammonium tropane 1,5-*syn*-triazole **4′** over the 1,4-*anti*-isomer **4** in the only instance in which activity was seen (Table 1; Supplemental Table 1).

In addition to receptor activities, Table 1 compares AChBP binding values reported previously (Grimster et al., 2012) for the 1,4-*anti*-triazoles (**1**-**5**), the 1,5-*syn*-triazoles (**1′**–**5′**), and triazole **6**, an initial product formed with the AChBPs. The tested receptor and AChBP activities of the quaternary amine 1,4-*anti*-triazoles (**7**-**9**), which were also generated through in situ synthesis (Grimster et al., 2012), are included in Table 1. Compounds **6** to **9** were found to be moderately potent agonists for $\alpha7$ nAChRs, with EC_{50} values comparable to those observed for **1** to **5**. Compounds **6**, **8**, and **9** were weak to moderate antagonists at $\alpha4\beta2$ nAChRs, whereas none of compounds **6** to **9** was active at 5-HT_{3A} receptors.

Compounds Generated with Partial *α7/A. californica* AChBP Chimera. Data for the initial in situ-generated compounds (**1**-**5**, **1′**–**5′**, and **6**-**9**) (Table 1; Supplemental Table 3) indicated that AChBPs might serve as promising templates for the generation of candidate $\alpha7$ nAChR-selective ligands. To identify selective and more-potent compounds for $\alpha7$ nAChRs, we performed an additional round of in situ click-chemistry reactions but used *A. californica* MT2 (Nemecz and Taylor, 2011), an available *A. californica* AChBP mutant with residues in the binding site mutated toward the human $\alpha7$ nAChR. To obtain *A. californica* MT2, mutations were made in the *A. californica* AChBP in loops B, D, and E but not loop C.

TABLE 1

Receptor and AChBP activities of in situ leads generated with *Aplysia californica* and *Lymnaea stagnalis* AChBPs, including cyclic quaternary amine quinolinone 1,4-anti- and 1,5-syn-triazoles and quaternary tropane 1,4-anti-triazoles with various aromatic groups attached through alkyne building blocks

Data include receptor functional activities (human $\alpha7$ nAChRs, human $\alpha4\beta2$ nAChRs, and mouse 5-HT_{3A} receptors) and AChBP dissociation constants for compounds generated in situ with wild-type *L. stagnalis*, *A. californica*, and *A. californica* Y55W AChBPs (**1**-**5**, **1′**–**5′**, and **6**-**9**). AChBP dissociation constants were calculated from scintillation proximity competition assays with (±)-[H^3]epibatidine. The structures and AChBP-binding properties of compounds **1** to **9** and **4′** were reported previously (Grimster et al., 2012). Antagonism of $\alpha4\beta2$ nAChRs showed mixed inhibition, but noncompetitive antagonist values were greater by factors of 1.3 to 20; therefore, inhibition was primarily competitive (both competitive and noncompetitive inhibition values are shown in Supplemental Table 2). Compounds with values represented as >30 μM were not identified as antagonists in screens (Supplemental Fig. 1). All values are reported as mean ± S.D. of the numbers of experiments in parentheses. Counter-ions shown as X^- in chemical structures differed between isomers and are listed in Supplemental Table 7. The full molecular structures for **4** and **4′** are shown in Figures 3 and 4.

Quinolinone Triazoles Formed with Azide R Groups 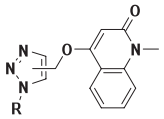	Agonist Activity at Human $\alpha7$, EC_{50}	Antagonist Activity, K_A		Binding to AChBPs, K_d		
		Human $\alpha4\beta2$	Mouse 5-HT_{3A}	*L. stagnalis*	*A. californica*	*A. californica* Y55W
	μM	μM		*nM*		
R Azides						
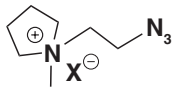						
1, *anti-*	3.7 ± 0.79 (5)	C, 20 ± 11 (3)	>30	18 ± 3.0 (3)	540 ± 77 (3)	62 ± 9.0 (3)
1′, *syn-*	6 ± 2.3 (6)	C, 30 ± 13 (3)	>30	60 ± 10 (3)	1400 ± 370 (3)	170 ± 30 (3)
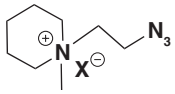						
2, *anti-*	1.2 ± 0.65 (6)	C, 12 ± 5.6 (3)	>30	10 ± 1.7 (3)	210 ± 46 (3)	50 ± 5.0 (3)
2′, *syn-*	4.2 ± 0.81 (6)	>30 (3)	>30	40 ± 15 (3)	800 ± 210 (3)	210 ± 60 (3)
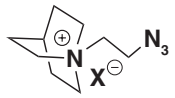						
3, *anti-*	1.8 ± 0.96 (4)	C, 8 ± 1.8 (3)	>30	9.0 ± 0.4 (3)	120 ± 25 (3)	88 ± 4.2 (3)
3′, *syn-*	2.9 ± 0.58 (7)	C, 30 ± 13 (3)	>30	24 ± 5.4 (3)	250 ± 80 (3)	290 ± 85 (3)
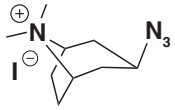						
4, *anti-*	0.3 ± 0.16 (6)	C, 4 ± 2.9 (3)	C, 34 ± 8.0 (3)	1.0 ± 0.22 (3)	24 ± 6.8 (3)	17 ± 4.8 (3)
4′, *syn-*	0.6 ± 0.12 (5)	C, 23 ± 5.6 (6)	C, 0.9 ± 0.40 (4)	2 ± 1.0 (3)	300 ± 110 (3)	100 ± 36 (3)
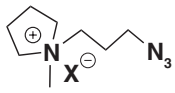						
5, *anti-*	0.8 ± 0.19 (6)	C, 18 ± 8.8 (3)	>30	80 ± 14 (3)	470 ± 65 (3)	280 ± 21 (3)
5′, *syn-*	2.0 ± 0.37 (6)	C, 40 ± 18 (3)	>30	600 ± 140 (3)	1400 ± 480 (3)	800 ± 210 (3)
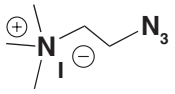						
6, *anti-*	1.7 ± 0.82 (6)	C, 14 ± 9.7 (3)	>30	80 ± 26 (3)	1900 ± 800 (3)	370 ± 50 (3)
Other Tropanes						
Triazoles						
7 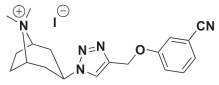	0.9 ± 0.38 (3)	>30	>30	40 ± 19 (3)	220 ± 87 (3)	130 ± 35 (3)
8 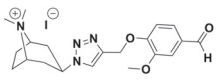	1.0 ± 0.45 (3)	C, 6 ± 2.9 (4)	>30	60 ± 26 (3)	260 ± 80 (3)	130 ± 44 (3)
9 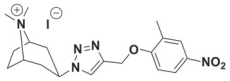	1.9 ± 0.54 (4)	C, 14 ± 8.9 (3)	>30	13 ± 6.5 (3)	60 ± 27 (3)	30 ± 18 (3)

C, competitive.

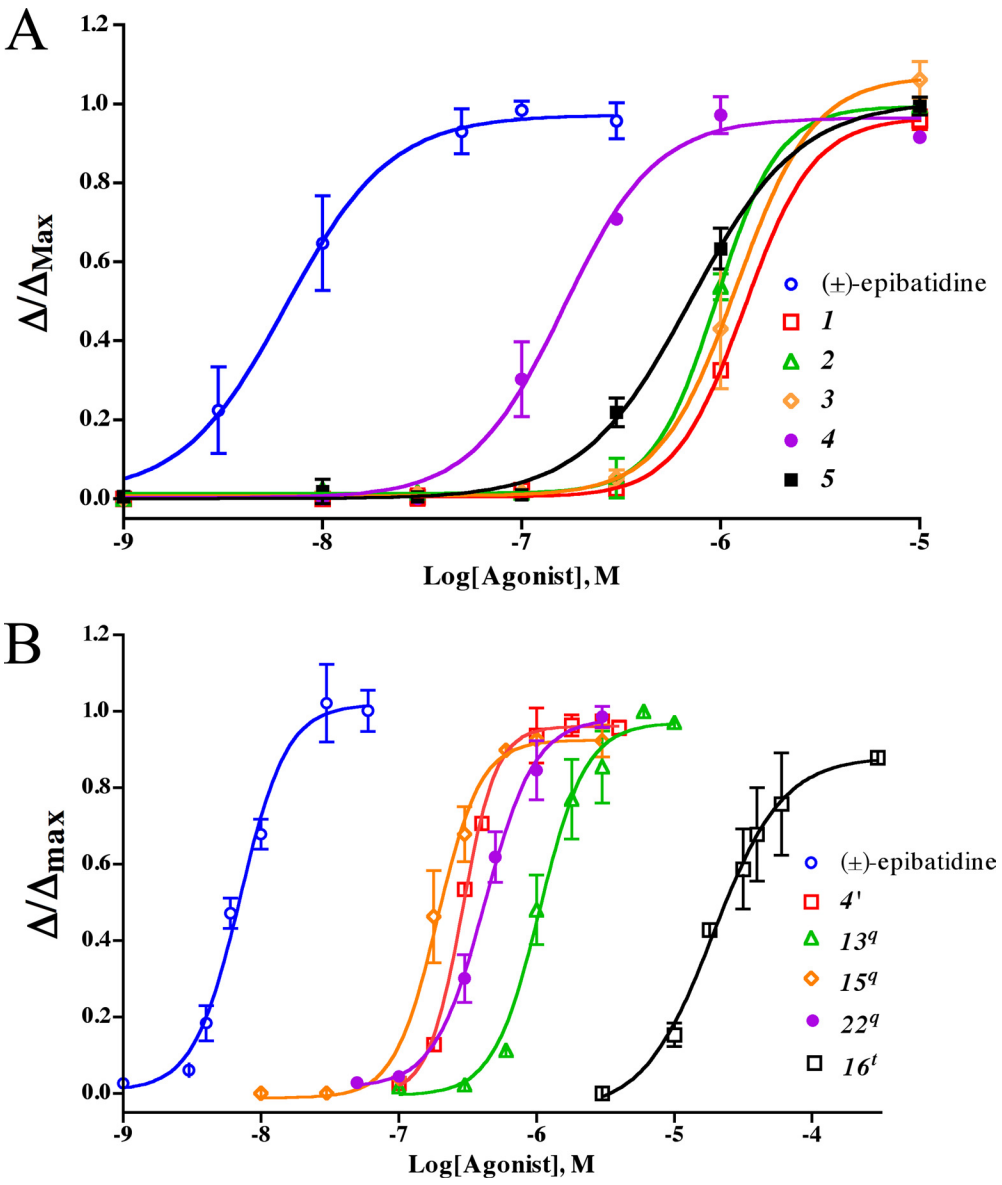

Fig. 1. Dose-response characterization of triazoles with human α7 nAChRs. Values were normalized (as fractions) to maximal values obtained for (±)-epibatidine at either 100 or 60 nM. A, of the 1,4-*anti*-triazoles (**1**–**5**) identified as agonists, triazole **4** found to have the highest potency (rank order: **4** > **5** > **2** ≥ **3** ≥ **1**). B, quaternary tropane triazoles were found to be more potent agonists than the tertiary forms (rank order: **15^q** > **4′** > **22^q** > **13^q** > **16^t**).

Among the 14 compounds described above, **4** and **4′** were determined to be the most potent for α7 nAChRs and contained the 3α-azido-*N*-methylammonium tropane building block moiety. Therefore, we used this azide building block to maintain potency for α7 nAChRs and screened 50 alkyne constituents to develop new selective triazoles (Supplemental Fig. 3). Because 1,4-*anti*-isomers typically exhibited lower EC_{50} values for α7 nAChRs and the 1,5-*syn*-isomer (**4′**) showed stronger inhibition of 5-HT_{3A} receptors than did the 1,4-*anti*-isomer (**4**), CuAAC was used to synthesize only the 1,4-*anti*-isomers of the compounds generated in situ with *A. californica* MT2.

Of the 50 alkyne building blocks that were reacted in situ with 3α-azido-*N*-methylammonium tropane with *A. californica* MT2 as a template, a total of 14 triazole products were identified and subsequently synthesized by using CuAAC (**10^q**-**23^q**). Pharmacological profiles for the assayed receptors are shown in Table 2. All 14 compounds were identified as MLA-sensitive agonists for α7 nAChRs (Supplemental Figs. 4A and 5), with **13^q**, **15^q**, **17^q**, **18^q**, and **22^q** exhibiting EC_{50} values of <1 μM (Table 2). The quaternary 2-(methylthio)-benzothiazole triazole (**15^q**) had the highest affinity for α7 nAChRs (EC_{50} = 0.20 μM); **15^q** was an antagonist for $\alpha4\beta2$ nAChRs but with 15-fold weaker antagonist activity, which reveals its α7 selectivity (competitive K_A = 3 μM; noncompetitive K_A = 8 μM) (Supplemental Table 4). All 14 of the quaternary compounds showed the trend of selectivity for α7 nAChRs, although **20^q** and **23^q** showed only 3.8-fold selectivity and the weak potency of **11^q** yielded minimal selectivity of ≥3-fold. The 1-(2-methoxynaphthalen-1-yl)ethanone triazole **22^q** was selected as a good lead compound on the basis of its selectivity and potency (EC_{50} = 0.4 μM) for α7 nAChRs. The triazoles **13^q**, **15^q**, **17^q**, and **18^q** were $\alpha4\beta2$ nAChR antagonists of moderate activity, with competitive K_A values of <10 μM, whereas **19^q**, **20^q**, **21^q**, and **23^q** were found to antagonize $\alpha4\beta2$ nAChRs weakly. Triazoles **15^q**, **17^q**, and **18^q** had similar, nearly equivalent, competitive and noncompetitive K_A values of <10 μM. Of the 14 triazoles, **17^q** was the only compound identified as an antagonist for 5-HT_{3A} receptors; it showed a dominant noncompetitive antagonism profile with a K_A of 8 μM (Fig. 5B).

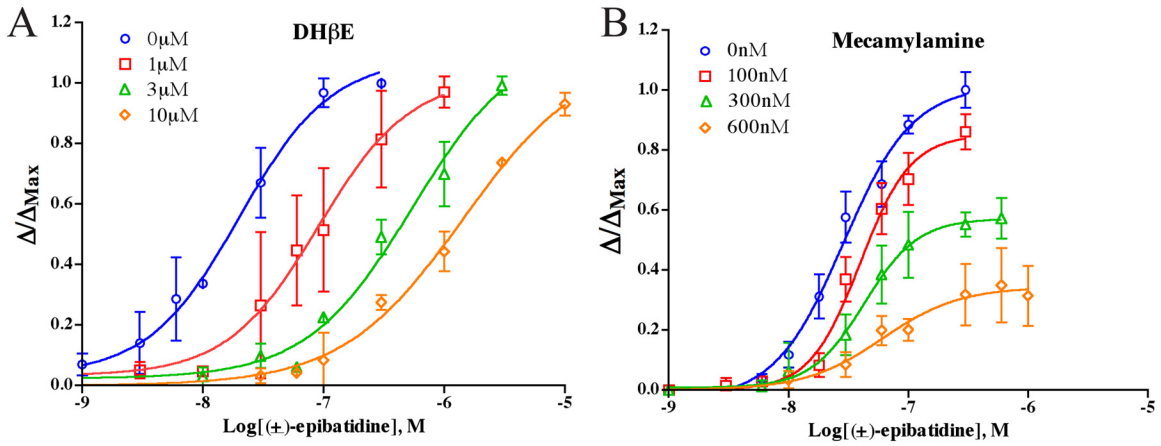

Fig. 2. Human $\alpha4\beta2$ nAChR competitive and noncompetitive antagonist profiles for dihydro-β-erythroidine (DHβE) and mecamylamine. Examples of competitive or noncompetitive inhibition from concentration-response profiles produced with varying concentrations of (±)-epibatidine are shown. A, inhibition of responses with dihydro-β-erythroidine produced classic competitive parallel shifts in EC_{50} values and the changes were surmountable with increased agonist concentrations; both characteristics indicate predominantly competitive behavior (competitive K_A = 300 ± 150 nM). Competitive K_A values were calculated from Schild plots by using dose ratios and the equation K_A = [A]/(DR − 1). B, mecamylamine inhibition produced minimal shifts in EC_{50} values with significant decreases in maximal responses, which are indicative of predominantly noncompetitive inhibition (noncompetitive K_A = 370 ± 60 nM).

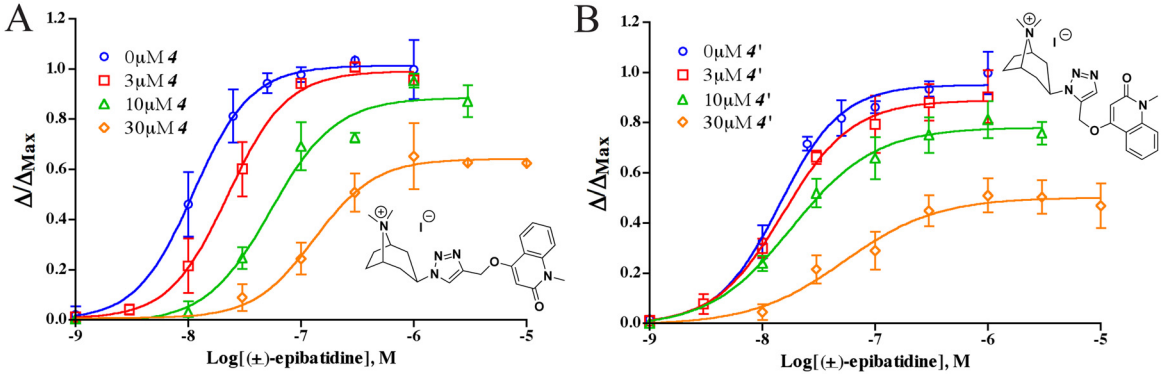

Fig. 3. Inhibition of human $\alpha4\beta2$ nAChRs with *N*-methylammonium tropane quinolinone triazole 1,4-*anti*- and 1,5-*syn*-isomers (**4** and **4′**). Concentration-response curves were generated with (±)-epibatidine in the presence or absence of identified antagonists, to yield inhibition constants and pharmacological profiles. A, the 1,4-*anti*-isomer **4** (K_A = 4 ± 2.9 μM) showed a potent competitive antagonist profile. B, the 1,5-*syn*-isomer **4′** (K_A = 23 ± 5.6 μM) was less potent than the 1,4-*anti*-isomer.

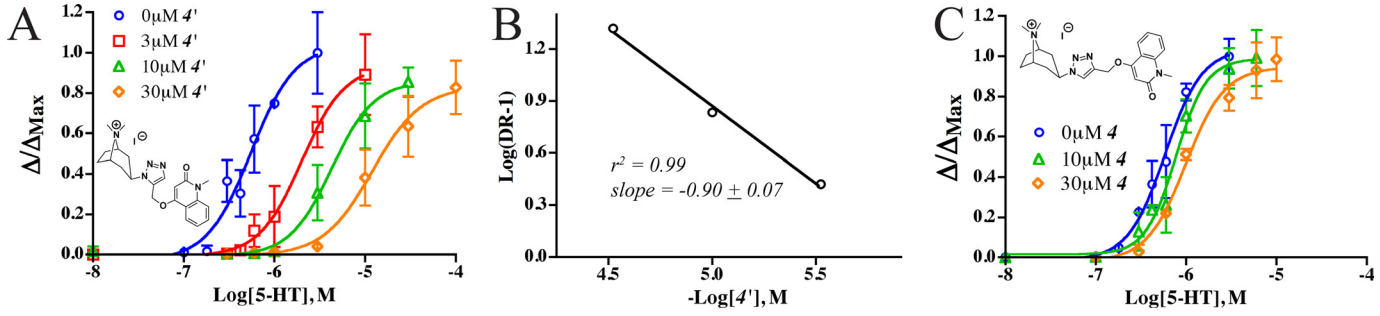

Fig. 4. Inhibition of mouse 5-HT_{3A} receptors with *N*-methylammonium tropane quinolinone triazole 1,4-*anti*- and 1,5-*syn*-isomers (**4** and **4′**). A, dose-response curves generated with 5-HT in the presence and absence of the quaternary tropane 1,5-*syn*-isomer **4′** indicated competitive antagonism, with parallel shifts in the EC_{50} values with increasing antagonist concentrations (K_A = 0.9 ± 0.4 μM). B, a Schild analysis of data for **4′** confirmed competitive inhibition, with a slope of −0.9. C, confirmation of low activity levels with the 1,4-*anti*-isomer **4** (K_A = 34 ± 8.0 μM) indicated a 38-fold decrease in affinity, compared with the 1,5-*syn*-isomer.

For assessment of the role of quaternization of the aza nitrogen in $\alpha7$ nAChR activation, the tertiary free-amine analog of **4** (**4^t**) and the 14 aforementioned 3α-azido-*N*-methylammonium tropane derivatives (**10^t**–**23^t**) were synthesized and then investigated for functional and binding activities with the receptors and AChBPs, respectively (Table 3). Only 5 of the 15 tropane triazole products (**4^t**, **15^t**, **16^t**, **20^t**, and **22^t**) were found to be agonists for $\alpha7$ nAChRs, because all tertiary analogs lost significant affinity, with none having an EC_{50} value below 1 μM. However, compound **16^t** maintained 6-fold selectivity for $\alpha7$ nAChRs. An increase in affinity with $\alpha4\beta2$ nAChRs was found for most of the tertiary analogs, with **10^t**, **12^t**, **14^t**, and **16^t** displaying weak antagonism, whereas their quaternary counterparts displayed no appre-

TABLE 2

Receptor activities of N-methylammonium tropane 1,4-anti-triazoles **(10[q]–23[q])** generated in situ with α7/AChBP partial chimera

All reported values are mean ± S.D. of the numbers of experiments in parentheses. Compounds with values represented as >30 μM were not identified in receptor screens (Supplemental Figure 4). Compounds with values represented as >5000 nM were not found to bind AChBPs (data not shown).

Quaternary Tropane 1,4-*anti*-Triazoles with Alkyne R Groups 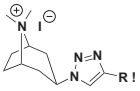	Agonist Activity at Human α7, EC_{50}	Antagonist Activity at Human α4β2, K_A	Binding to AChBPs, K_d				
			Mouse 5-HT_{3A}	*Lymnaea stagnalis*	*Aplysia californica*	*A. californica* Y55W	*A. californica* MT2
	μM	*μM*			*nM*		
4 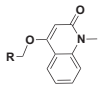	0.3 ± 0.16 (6)	C, 4 ± 2.9 (3); NC, 60 ± 13 (3)	C, 34 ± 7.8 (3)	1.0 ± 0.22 (3)	24 ± 6.8 (3)	17 ± 4.8 (3)	40 ± 17 (3)
10[q] 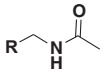	5 ± 3.0 (7)	>30	>30	>5000	800 ± 310 (3)	>5000	900 ± 150 (3)
11[q] 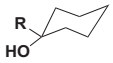	9 ± 2.0 (4)	>30	>30	>5000	>5000	>5000	50 ± 19 (3)
12[q] 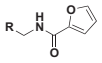	3 ± 1.8 (9)	>30	>30	400 ± 190 (4)	600 ± 260 (3)	1000 ± 150 (3)	700 ± 270 (3)
13[q] 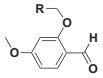	0.8 ± 0.46 (11)	C, 7 ± 2.8 (4); NC, 19 ± 4.4 (4)	>30	20 ± 16 (3)	110 ± 30 (3)	120 ± 70 (3)	80 ± 24 (3)
14[q] 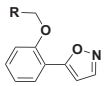	2 ± 1.0 (7)	>30	>30	50 ± 15 (3)	140 ± 74 (3)	170 ± 85 (3)	96 ± 8.5 (3)
15[q] 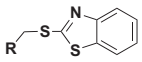	0.20 ± 0.068 (10)	C, 3 ± 1.7 (4); NC, 8 ± 3.8 (4)	>30	4 ± 1.3 (3)	13 ± 6.9 (3)	13 ± 4.4 (3)	8 ± 1.1 (3)
16[q] 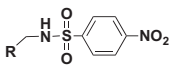	1.8 ± 0.85 (8)	>30	>30	>5000	620 ± 94 (3)	800 ± 420 (3)	600 ± 180 (3)
17[q] 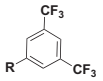	0.9 ± 0.25 (9)	C, 5 ± 2.4 (4); NC, 5 ± 2.0 (4)	C, 50 ± 14 (3); NC, 8 ± 1.1 (3)	130 ± 62 (3)	110 ± 20 (3)	300 ± 140 (3)	400 ± 100 (3)
18[q] 	0.4 ± 0.28 (9)	C, 4 ± 1.3 (5); NC, 8 ± 3.0 (5)	>30	70 ± 32 (3)	260 ± 52 (3)	270 ± 54 (3)	440 ± 89 (3)
19[q] 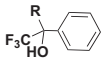	2 ± 1.1 (8)	C, 22 ± 4.7 (4); NC, 41 ± 7.2 (4)	>30	120 ± 29 (3)	800 ± 460 (3)	>5000	60 ± 27 (3)
20[q] 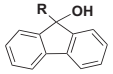	4 ± 2.5 (10)	C, 15 ± 5.7 (5); NC, 23 ± 5.6 (5)	>30	50 ± 28 (3)	400 ± 100 (3)	600 ± 280 (4)	120 ± 48 (3)
21[q] 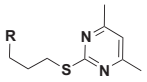	3 ± 1.4 (9)	C, 60 ± 32 (2); NC, 27.1 ± 0.19 (2)	>30	40 ± 18 (3)	18 ± 7.8 (3)	30 ± 17 (3)	400 ± 110 (3)
22[q] 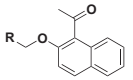	0.4 ± 0.22 (10)	>30	>30	160 ± 57 (3)	200 ± 82 (3)	300 ± 150 (3)	900 ± 260 (3)
23[q] 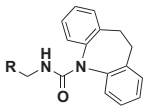	8 ± 3.6 (9)	C, 30 ± 21 (4); NC, 40 ± 18 (4)	>30	500 ± 200 (3)	420 ± 43 (3)	1000 ± 300 (3)	2000 ± 700 (3)

C, competitive; NC, noncompetitive.

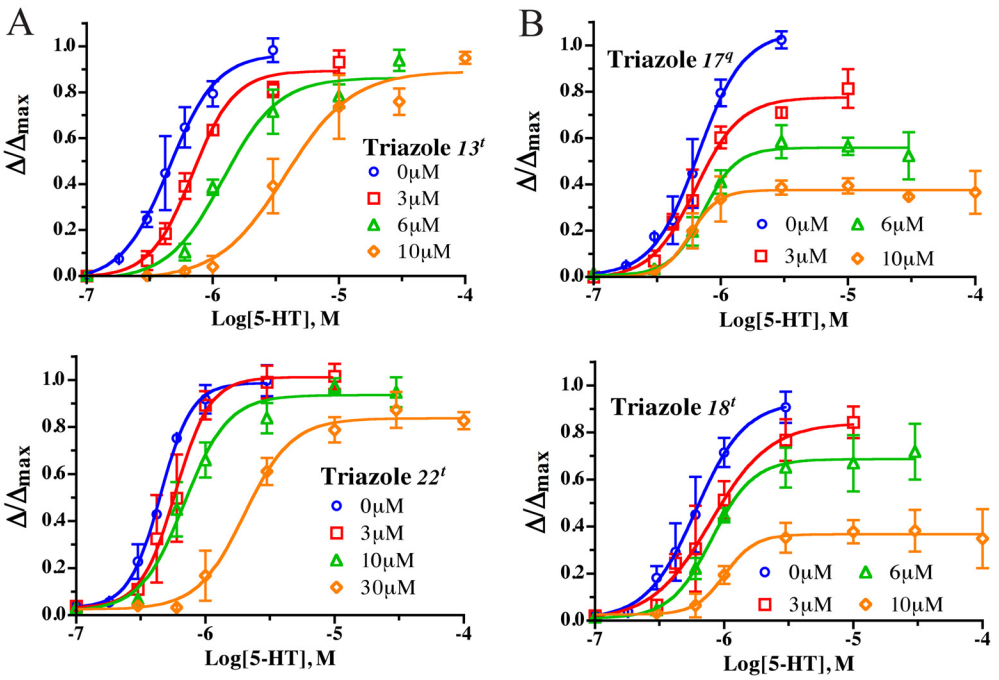

Fig. 5. Inhibition of mouse 5-HT_{3A} receptors with compounds generated in situ with *A. californica* MT2 AChBP. Dose-response curves for 5-HT in the presence and absence of identified antagonists produced inhibition constants for slightly different modes of inhibition. For each set of curves, independent measurements of 5-HT concentration-dependent responses without antagonist were used as reference curves (Hill slopes ranged from 2 to ~3). A, competitive profiles were observed for triazoles **13**^{t} and **22**^{t}. Competitive K_A values were 5 ± 1.4 and 12 ± 1.4 μM, respectively. B, mixed or noncompetitive profiles were obtained for triazoles **17**^{q} and **18**^{t}. Noncompetitive K_A values were 8 ± 1.1 and 14 ± 3.2 μM, respectively.

ciable antagonism. Triazole **13**^{t} switched the dominant mechanism of action from a competitive mode of inhibition to noncompetitive, whereas **21**^{t} switched from noncompetitive to competitive, and both increased overall potency. Triazoles **15**^{t} and **18**^{t} maintained moderate antagonism and behavior for α4β2 nAChRs, with **22**^{t} increasing its affinity to behave like **15**^{t} and **18**^{t}, with nearly equivalent measured competitive and noncompetitive K_A values of <10 μM. Compounds **20**^{t} and **23**^{t} also maintained their behavior, displaying similar weak antagonism, whereas triazoles **4**^{t}, **17**^{t}, and **19**^{t} were the only triazoles to lose affinity for α4β2 nAChRs. More tertiary than quaternary triazole compounds were active at 5-HT_{3A} receptors (Supplemental Table 4); these typically had greater potency and showed competitive inhibition profiles (Fig. 5A). The tertiary compounds identified as antagonists for 5-HT_{3A} receptors were **4**^{t}, **13**^{t}, **15**^{t}, **18**^{t}, and **22**^{t}. Changing the tertiary tropane amine to a quaternary amine affected the noncompetitive component significantly for 5-HT_{3A} receptors, whereas the weak competitive component was hardly affected (Table 3). The tertiary analogs **13**^{t} and **22**^{t} exhibited moderate competitive inhibition of 5-HT_{3A} receptors (Fig. 5A). For **15**^{t}, however, competitive inhibition was less pronounced. Triazole **18**^{t} had weak but similar, nearly equivalent, competitive and noncompetitive components of inhibition with 5-HT_{3A} receptors (Fig. 5B; Table 3).

Discussion

Leads Generated with In Situ Click-Chemistry Methods. In this study and a previous analysis (Grimster et al., 2012), we established that in situ click-chemistry methods can be used to generate new leads for pharmacological receptors, by using surrogate AChBPs as soluble templates for synthesis. Therefore, template applicability was expanded from well defined and partially sequestered sites within enzyme subunits to a subunit interface on a multisubunit protein.

In contrast to traditional, fragment-based, drug design, the in situ approach allows the target template to drive synthetic preferences by selecting combinations of building blocks that best occupy the active site; this was demonstrated with a minimal set by using acetylcholinesterase (Lewis et al., 2002) and now by using AChBP for more-diverse building block arrays. The amount of product formed in situ correlated with the overall affinity of the complex formed on the target surface (Grimster et al., 2012). In previous work (Lewis et al., 2002; Bourne et al., 2004, 2010b), the in situ click-chemistry approach was shown to select minor-abundance conformations with higher affinities for the triazole generated than for the predominant unliganded conformation. Therefore, click-chemistry reactions freeze in-frame template conformations that prefer formation of the complex. This conformational selection is based solely on ligand affinity, however, and does not distinguish agonist from antagonist activity.

Selectivity for nAChRs and AChBPs. Our functional pLGIC receptor studies with α7 nAChR lead compounds that were generated in situ with different AChBP templates revealed findings critical to the expanding applications of the in situ click-chemistry approach and identified ligand determinants that confer α7 nAChR selectivity. With previously generated in situ compounds (**1**-**9** and **1′**–**5′**), we identified 1,4-*anti*-triazole as the preferred regioisomer for α7 nAChRs, because of its observed potency and lack of 5-HT_{3A} receptor activity, as evident with the 1,5-*syn*-triazole **4′** (Table 1). We chose a lead azide building block, 3α-azido-*N*-methylammonium tropane (Grimster et al., 2012), because triazole **4** had the highest α7 nAChR affinity (Table 1).

We hypothesized that the products formed on the *A. californica* MT2 template (Nemecz and Taylor, 2011), which more closely replicates α7 nAChR, would exhibit enhanced α7 nAChR affinity and would confer additional selectivity. Chemical refinement of the alkyne termini resulted in 14 triazole products (**10**^{q}–**23**^{q}) formed from 50 alkyne building blocks (Supplemental Fig. 4) that had been allowed to react in situ with the 3α-azido-*N*-methylammonium tropane. All 14 products were functionally selective as α7 nAChR ago-

TABLE 3

Functional activities at receptors and dissociation constants at AChBPs for tertiary tropane 1,4-anti-triazole analogs (**4^t** and **10^t–23^t**) generated through Cu(I) catalysis

All reported values are mean ± S.D. of the numbers of experiments in parentheses. Compounds with values represented as >30 μM were not identified in receptor screens (Supplemental Fig. 4); those with values of >5000 nM were not found to bind AChBPs (data not shown).

Tertiary Tropane 1,4-*anti*-Triazoles with Alkyne R Groups 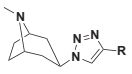	Agonist Activity at Human α7, EC_{50}	Antagonist Activity at Human α4β2, K_A	Binding to AChBPs, K_d				
			Mouse 5-HT_{3A}	*Lymnaea stagnalis*	*Aplysia californica*	*A. californica* Y55W	*A. californica* MT2
	μM	*μM*			*nM*		
4^t 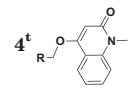	11 ± 6.1 (5)	C, 14 ± 9.7 (3)	C, 15 ± 1.5 (3)	1.30 ± 0.011 (3)	109 ± 2.8 (3)	16 ± 1.7 (3)	600 ± 150 (3)
10^t 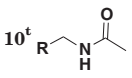	>30	C, 18 ± 8.3 (3); NC, 29 ± 3.7 (3)	>30	900 ± 120 (3)	>5000	>5000	>5000
11^t 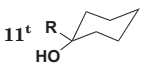	>30	>30	>30	>5000	>5000	>5000	>5000
12^t 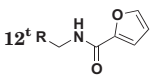	>30	C, 30 ± 19 (3); NC, 20 ± 11 (3)	>30	210 ± 78 (3)	>5000	1400 ± 520 (3)	>5000
13^t 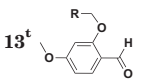	>30	C, 20 ± 15 (4); NC, 6 ± 3.8 (5)	C, 5 ± 1.4 (3)	26 ± 8.2 (3)	1200 ± 360 (3)	390 ± 49 (3)	>5000
14^t 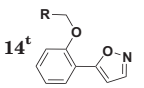	>30	C, 16 ± 9.0 (4); NC, 13 ± 5.2 (4)	>30	25 ± 4.1 (3)	500 ± 210 (3)	300 ± 120 (3)	>5000
15^t 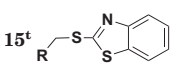	12 ± 2.1 (3)	C, 8 ± 6.5 (2); NC, 4 ± 2.8 (3)	C, 32 ± 8.5 (3)	40 ± 16 (3)	240 ± 82 (3)	140 ± 59 (3)	110 ± 48 (3)
16^t 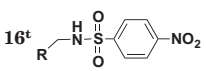	5 ± 1.8 (4)	C, 60 ± 27 (3); NC, 30 ± 16 (5)	>30	>5000	>5000	>5000	>5000
17^t 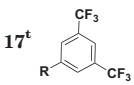	>30	>30	>30	600 ± 190 (3)	1100 ± 270 (3)	>5000	>5000
18^t 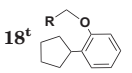	>30	C, 5 ± 1.8 (4); NC, 3 ± 1.8 (4)	C, 12 ± 2.8 (3); NC, 14 ± 3.2 (3)	30 ± 7.7 (3)	900 ± 220 (3)	370 ± 50 (3)	>5000
19^t 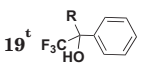	>30	C, 80 ± 53 (3); NC, 40 ± 21 (3)	>30	>5000	>5000	>5000	>5000
20^t 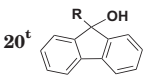	12 ± 6.1 (3)	C, 17 ± 7.5 (3); NC, 39 ± 2.0 (3)	>30	500 ± 200 (4)	2000 ± 130 (3)	3100 ± 460 (3)	>5000
21^t 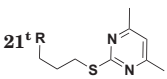	>30	C, 10 ± 12 (3); NC, 20 ± 10 (3)	>30	300 ± 110 (3)	360 ± 40 (3)	560 ± 80 (3)	>5000
22^t 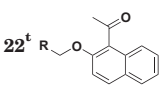	9 ± 1.1 (3)	C, 5 ± 2.5 (5); NC, 4 ± 1.6 (5)	C, 12 ± 1.4 (3)	141 ± 8.3 (3)	800 ± 120 (3)	700 ± 100 (3)	>5000
23^t 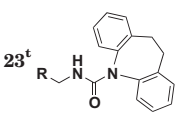	>30	C, 20 ± 5.7 (2); NC, 13 ± 4.3 (3)	>30	>5000	1300 ± 400 (3)	1020 ± 72 (3)	>5000

C, competitive; NC, noncompetitive.

nists, with five (**13^q**, **15^q**, **17^q**, **18^q**, and **22^q**) exhibiting EC_{50} values below 1 μM, whereas eight (**13^q**, **15^q**, **17^q**, **18^q**, **19^q**, **20^q**, **21^q**, and **23^q**) showed $\alpha4\beta2$ antagonism. Eleven of the 14 triazoles generated were ≥5-fold selective for $\alpha7$ nAChRs (**11^q**, **20^q**, and **23^q** were the exceptions, with the poor affinity of **11^q** limiting the selectivity determination), and one (**22^q**) was both potent and ≥75-fold selective (Table 2; Supplemental Table 4). The quaternary in situ agonists for $\alpha7$ nAChRs showed greater selectivity relative to 5-HT_{3A} receptors than $\alpha4\beta2$ nAChRs (Supplemental Table 4), an expectation arising from greater conservation of aromatic residues in the nAChR binding site.

Our comparison of tertiary (**4^t** and **10^t**–**23^t**) and quaternary (**4** and **10^q**–**23^q**) 1,4-*anti*-triazoles showed large reductions in $\alpha7$ nAChR activity with replacement of the quaternized nitrogen. Five of the tertiary amine analogs (**4^t**, **15^t**, **16^t**, **20^t**, and **22^t**) were detected as $\alpha7$ nAChR agonists, but none was highly selective (Supplemental Table 6). The lower activity of these tertiary tropane triazoles represents a limitation, because a fractional unprotonated (neutral) amine species is required for crossing the blood-brain barrier for candidate CNS therapeutic agents. However, quaternary compounds offer unique therapeutic opportunities to target $\alpha7$ nAChRs outside the CNS, e.g., control of peripheral inflammation (de Jonge and Ulloa, 2007).

All products were $\alpha7$ nAChR agonists and contained the aza nitrogen moiety of the *N*-methylammonium tropane, as well as short links to either an aromatic or aliphatic group with weak hydrogen bond acceptor capacity. The most potent and selective compound, triazole **22^q**, features a positively charged *N*-methylammonium tropane and aromatic methyleneoxynaphthylenethanone. The other products formed revealed pharmacophore models for leads that were consistent with studies on $\alpha7$ nAChRs (Horenstein et al., 2008), which demonstrated the recognition capacity of the template to select preferred binding partners.

Structural Insights into $\alpha7$ nAChR Selectivity from AChBP Data. The most potent triazoles for $\alpha7$ nAChRs were the *N*-methylammonium tropane 1,4-*anti*-triazoles and, given the structural similarities among them, all compounds were predicted to bind in similar configurations to a common receptor or binding protein, as shown in the *A. californica* AChBP complex with **4** (Fig. 6), which was previously referred to as **18** [Protein Data Bank (PDB) no. 4DBM] (Grimster et al., 2012). This structure reveals potential cation-π interactions (Dougherty, 1996) between the quaternary nitrogen and the π-orbitals of a group of aromatic side chains in the receptor binding pocket (Xiu et al., 2009; Blum et al., 2010; Puskar et al., 2011) as dominant contributors to the stability of the complex (Fig. 6A). The α-subunit aromatic side chains Tyr93, Trp147, Tyr188, and Tyr195, in addition to either Tyr55 or Trp55 on the complementary face, are all conserved in AChBPs and in $\alpha7$ and $\alpha4\beta2$ nAChRs.

Stabilization of tertiary amine complexes differs when stabilization is conferred through a protonated amine and donation of a hydrogen bond to the backbone carbonyl group of Trp147, as reported for AChBP complexes with nicotine (PDB no. 1UW6) (Celie et al., 2004), epibatidine (PDB no. 2BYQ) (Hansen et al., 2005), and the tertiary tropane tropisetron (PDB 2WNC) (Hibbs et al., 2009). A similar situa-

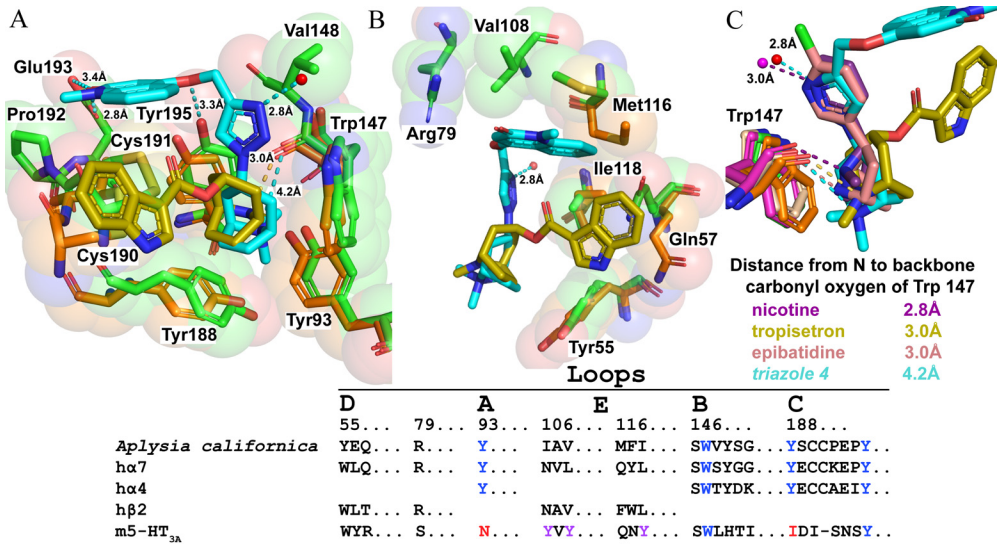

Fig. 6. Crystallographic configuration of triazole **4** (quaternary tropane) overlaid with those of tropisetron (tertiary tropane), nicotine, and epibatidine complexes with *A. californica* and *L. stagnalis* AChBPs. A and B, primary face (A) and complementary face (B) residues from overlaid structures of triazole **4** (PDB no. 4DBM) (cyan), previously referred to as **18** (Grimster et al., 2012), and tropisetron (PDB no. 2WNC) (mustard) (Hibbs et al., 2009), both in complex with *A. californica* AChBP. The residues shown in stick form are within 4 Å of the ligands (green, triazole **4**; orange, tropisetron). Polar contacts for each ligand are colored accordingly, with an additional representation of the distance from the quaternary nitrogen in **4** to the backbone carbonyl of Trp147 indicating proximity to and potential cation-π interaction with the aromatic indole side chain. C, additional ligand overlay of complexes including nicotine (plum) in *L. stagnalis*-AChBP (magenta) (Celie et al., 2004) and epibatidine (salmon) in *A. californica* AChBP (beige) (Hansen et al., 2005) (PDB nos. 1UW6 and 2BYQ, respectively). Triazole **4** and tropisetron are colored as in A and B. Nitrogen atom distances from the quaternary tropane of **4**, the tertiary tropane of tropisetron, the pyrolidine of nicotine, and the azabicyloheptane of epibatidine to the backbone carbonyl oxygen of Trp147 are shown. A hydrogen bond between the N3 atom of triazole **4** and a water molecule (red sphere) is comparable to the hydrogen bond between water (magenta sphere) and the pyridine ring of nicotine. Also shown is a sequence alignment of the relevant residues (and interconnecting residues) listed in each subunit. Blue-highlighted residues are conserved aromatic residues in the primary subunit (loops A, B, and C). Red-highlighted residues are changes in the 5-HT_{3A} receptor primary subunit, in which two key aromatic residues are lost, compared with *A. californica* AChBP and nAChRs (Tyr93 and Tyr188). Purple-highlighted residues are changes in the 5-HT_{3A} receptor complementary subunit (loops D and E), which contains aromatic tyrosine residues at positions 106, 108, and 118 that are not found in *A. californica* AChBP and nAChRs.

tion arises for protonated imines in anabaseine analogs and macrocyclic dinoflagelate toxins (Hibbs et al., 2009; Bourne et al., 2010a). The protonated nitrogen is appropriately oriented within hydrogen bonding distances (2.9–3.1 Å) from the amide backbone carbonyl of Trp147. The structures reveal a 1.2-Å difference (4.2 vs. 3.0 Å) between the quaternary and tertiary nitrogen positions of the tropane amines (Fig. 6A).

In the presumed binding site at the subunit interface of the 5-HT_{3A} receptor, Tyr93 is replaced by Asn and Tyr188 by Ile (Fig. 6A). Moreover, the complementary subunit face possesses aromatic side chains (Tyr106, Tyr108, and Tyr118) that are not found in AChBPs or nAChRs. This altered position of aromatic side chains may explain the 5-HT_{3A} receptor preference for tertiary over quaternary tropanes and may suggest an inverted ligand configuration.

The triazole ring was found to be partially occluded, with its ring carbons facing outward from the pore toward the vicinal Cys190 and Cys191 in loop C (Fig. 6A). The triazole nitrogen N3 of **4** is oriented toward the complementary subunit, occupying positions identical to those of the pyridine nitrogens in epibatidine and nicotine, with the formation of a hydrogen bond to a water molecule (Fig. 6C). The overlay of the third ring system shows a major difference in the positioning of the quinolinone ring in **4** and the indole ring in tropisetron.

Our functional studies with the triazole compounds revealed two response modes for nAChR subtypes, i.e., agonists for the $\alpha7$ nAChR and antagonists for the $\alpha4\beta2$ nAChR. Studies using unnatural amino acids found that these receptors revealed different energy contributions among the aromatic side chains (Xiu et al., 2009; Blum et al., 2010; Puskar et al., 2011). A stronger cation-π interaction at Trp147 was evident for $\alpha4\beta2$ nAChR sites, compared with $\alpha7$ nAChR sites, whereas $\alpha7$ nAChR sites form strong cation-π interactions at Tyr195. The strength of the hydrogen bond formed at the backbone carbonyl of Trp147 is strong for $\alpha4\beta2$ nAChRs but moderate for $\alpha7$ nAChRs, which explains the tertiary preference for $\alpha4\beta2$ nAChRs. These results, along with our findings of distinct agonist ($\alpha7$ nAChR) and antagonist ($\alpha4\beta2$ nAChR) actions of the *N*-methylammonium tropane triazoles, reveal clear distinctions in binding modes between the $\alpha7$ and $\alpha4\beta2$ nAChRs and suggest that occupation and activation of nAChRs result from distinct configurations of the triazole ligand on $\alpha7/\alpha7$ versus $\alpha4/\beta2$ principal/complementary subunit interfaces.

Refinement of Leads for nAChRs. Leads generated through the in situ click-chemistry approach are limited by the template structure and conformation upon which the triazoles are generated. Although they possess shared recognition capacities common for neurotransmitters and an array of peptide, alkaloid, and terpene toxins, the structurally homologous AChBPs and nAChRs demonstrate several distinct characteristics. First, although AChBPs exist in select invertebrate species (Smit et al., 2001; Hansen et al., 2004; Celie et al., 2005; Huang et al., 2009; McCormack et al., 2010), evolutionary distances impart substantial sequence differences, compared with human nAChRs. Second, ligand binding to AChBPs is described by a simple adsorption isotherm and does not show cooperativity, as seen for nAChRs, which is indicative of multiple protein states (Hansen et al., 2004); interconversion of conformational states of nAChRs governed by the ligand is not evident for AChBPs. Third, refined analysis of selectivities for an increasing variety of ligands indicated that AChBPs, similar to receptor subtypes, had species-specific recognition properties that were not replicated with a single receptor subtype (Hansen et al., 2005; Talley et al., 2006; Hibbs et al., 2009; Rucktooa et al., 2009).

To overcome the limitations of the AChBP templates for nAChR ligand generation, we considered two approaches to enhance selectively. In a previous study, the *A. californica* and *L. stagnalis* AChBPs were mutated to become more $\alpha7$-like in sequence, particularly around the interfacial binding site (Nemecz and Taylor, 2011). The enhanced selectivity conferred by the modified binding site is limited because AChBP folding does not tolerate several mutations. Although the $\alpha7$ nAChR template (*A. californica* MT2) is far from a precise replicate of the receptor target, products generated in situ offer insights into the chemical landscape around the template pocket, which resembles the $\alpha7$ nAChR. Another approach is to examine selectivity in structural terms by using congeneric ligands in complexes with various AChBPs, particularly with mutants that resemble human receptors. As these complexes become available, classification of binding configurations with chemical groupings of agonists and antagonists may facilitate elucidation of the mechanisms of nAChR selectivity.

We characterized leads in which heterocyclic amines were modified, and we identified 3α-azido-*N*-methylammonium tropane as a potent $\alpha7$ nAChR building block lead. By using functional receptor assays, rapid determination of pharmacological activities (agonist or antagonist) is possible for pLGIC receptors, which enables ranking of potencies of in situ leads generated at AChBP templates. A logical extension of in situ screening entails refinement through synthetic modifications of identified in situ leads, such as triazole **22^{q}**, to enlarge the ligand base through Cu(I)- and Ru(II)-catalyzed synthetic reactions.

In summary, the click-chemistry approach with in situ-generated leads, followed by catalytic syntheses, presents a novel efficient tool for drug discovery, by decreasing the time and materials required to identify the chemical space surrounding a protein recognition site. In cases in which the drug target is limited by its expression in soluble form, we showed that soluble surrogates can be used as in situ templates and lead compounds can transition from possessing affinity at the soluble template (AChBP) to demonstrating agonist/antagonist activity at receptors. We demonstrated here two independent approaches to address structure refinements to enhance selectivity. The first involves conversion of the template through mutagenesis to become more receptor-like in sequence, whereas the second entails catalytic synthesis of congeners of the leads. An inherent advantage of soluble templates is the opportunity for structural characterization of lead-target complexes, to define the design base. The potential is not yet fully realized but, as more structures become available, template and ligand structure modifications should lead to more-rigorous design constraints.

Acknowledgments

Special thanks go to Jean-Pierre Changeux for insightful and provocative discussions. We acknowledge Wenru Yu for her expertise in tissue culture and protein purification.

Authorship Contributions

Participated in research design: Yamauchi, Grimster, Nemecz, Talley, Sharpless, Fokin, and Taylor.

Conducted experiments: Yamauchi, Gomez, Grimster, Dufouil, Fotsing, and Ho.

Contributed new reagents or analytic tools: Yamauchi, Grimster, Dufouil, Nemecz, Talley, Sharpless, Fokin, and Taylor.

Performed data analysis: Yamauchi, Gomez, Grimster, Dufouil, Nemecz, Fotsing, Ho, Talley, Sharpless, Fokin, and Taylor.

Wrote or contributed to the writing of the manuscript: Yamauchi, Grimster, Nemecz, Fotsing, Sharpless, Fokin, and Taylor.

References

Arunlakshana O and Schild HO (1959) Some quantitative uses of drug antagonists. *Br J Pharmacol Chemother* **14:**48–58.

Blum AP, Lester HA, and Dougherty DA (2010) Nicotinic pharmacophore: the pyridine N of nicotine and carbonyl of acetylcholine hydrogen bond across a subunit interface to a backbone NH. *Proc Natl Acad Sci USA* **107:**13206–13211.

Bourne Y, Kolb HC, Radić Z, Sharpless KB, Taylor P, and Marchot P (2004) Freeze-frame inhibitor captures acetylcholinesterase in a unique conformation. *Proc Natl Acad Sci USA* **101:**1449–1454.

Bourne Y, Radic Z, Aráoz R, Talley TT, Benoit E, Servent D, Taylor P, Molgó J, and Marchot P (2010a) Structural determinants in phycotoxins and AChBP conferring high affinity binding and nicotinic AChR antagonism. *Proc Natl Acad Sci USA* **107:**6076–6081.

Bourne Y, Radić Z, Taylor P, and Marchot P (2010b) Conformational remodeling of femtomolar inhibitor-acetylcholinesterase complexes in the crystalline state. *J Am Chem Soc* **132:**18292–18300.

Brejc K, van Dijk WJ, Klaassen RV, Schuurmans M, van Der Oost J, Smit AB, and Sixma TK (2001) Crystal structure of an ACh-binding protein reveals the ligand-binding domain of nicotinic receptors. *Nature* **411:**269–276.

Celie PH, Klaassen RV, van Rossum-Fikkert SE, van Elk R, van Nierop P, Smit AB, and Sixma TK (2005) Crystal structure of acetylcholine-binding protein from *Bulinus truncatus* reveals the conserved structural scaffold and sites of variation in nicotinic acetylcholine receptors. *J Biol Chem* **280:**26457–26466.

Celie PH, van Rossum-Fikkert SE, van Dijk WJ, Brejc K, Smit AB, and Sixma TK (2004) Nicotine and carbamylcholine binding to nicotinic acetylcholine receptors as studied in AChBP crystal structures. *Neuron* **41:**907–914.

de Jonge WJ and Ulloa L (2007) The alpha7 nicotinic acetylcholine receptor as a pharmacological target for inflammation. *Br J Pharmacol* **151:**915–929.

Dougherty DA (1996) Cation-pi interactions in chemistry and biology: a new view of benzene, Phe, Tyr, and Trp. *Science* **271:**163–168.

Grimster NP, Stump B, Fotsing JR, Weide T, Talley TT, Yamauchi JG, Nemecz Á, Kim C, Ho KY, Sharpless KB, et al. (2012) Generation of candidate ligands for nicotinic acetylcholine receptors via in situ click chemistry with a soluble acetylcholine binding protein template. *J Am Chem Soc* **134:**6732–6740.

Hansen SB, Sulzenbacher G, Huxford T, Marchot P, Taylor P, and Bourne Y (2005) Structures of *Aplysia* AChBP complexes with nicotinic agonists and antagonists reveal distinctive binding interfaces and conformations. *EMBO J* **24:**3635–3646.

Hansen SB, Talley TT, Radic Z, and Taylor P (2004) Structural and ligand recognition characteristics of an acetylcholine-binding protein from *Aplysia californica*. *J Biol Chem* **279:**24197–24202.

Hibbs RE, Sulzenbacher G, Shi J, Talley TT, Conrod S, Kem WR, Taylor P, Marchot P, and Bourne Y (2009) Structural determinants for interaction of partial agonists with acetylcholine binding protein and neuronal α7 nicotinic acetylcholine receptor. *EMBO J* **28:**3040–3051.

Horenstein NA, Leonik FM, and Papke RL (2008) Multiple pharmacophores for the selective activation of nicotinic α7-type acetylcholine receptors. *Mol Pharmacol* **74:**1496–1511.

Huang J, Wang H, Cui Y, Zhang G, Zheng G, Liu S, Xie L, and Zhang R (2009) Identification and comparison of amorphous calcium carbonate-binding protein and acetylcholine-binding protein in the abalone, *Haliotis discus hannai*. *Mar Biotechnol (NY)* **11:**596–607.

Karlin A (2002) Emerging structure of the nicotinic acetylcholine receptors. *Nat Rev Neurosci* **3:**102–114.

Kenney JW and Gould TJ (2008) Modulation of hippocampus-dependent learning and synaptic plasticity by nicotine. *Mol Neurobiol* **38:**101–121.

Kolb HC and Sharpless KB (2003) The growing impact of click chemistry on drug discovery. *Drug Discov Today* **8:**1128–1137.

Kuryatov A, Luo J, Cooper J, and Lindstrom J (2005) Nicotine acts as a pharmacological chaperone to up-regulate human $\alpha4\beta2$ acetylcholine receptors. *Mol Pharmacol* **68:**1839–1851.

Lewis WG, Green LG, Grynszpan F, Radić Z, Carlier PR, Taylor P, Finn MG, and Sharpless KB (2002) Click chemistry in situ: acetylcholinesterase as a reaction vessel for the selective assembly of a femtomolar inhibitor from an array of building blocks. *Angew Chem Int Ed Engl* **41:**1053–1057.

Majireck MM and Weinreb SM (2006) A study of the scope and regioselectivity of the ruthenium-catalyzed [3 + 2]-cycloaddition of azides with internal alkynes. *J Org Chem* **71:**8680–8683.

Mank M, Santos AF, Direnberger S, Mrsic-Flogel TD, Hofer SB, Stein V, Hendel T, Reiff DF, Levelt C, Borst A, et al. (2008) A genetically encoded calcium indicator for chronic in vivo two-photon imaging. *Nat Methods* **5:**805–811.

McCormack T, Petrovich RM, Mercier KA, DeRose EF, Cuneo MJ, Williams J, Johnson KL, Lamb PW, London RE, and Yakel JL (2010) Identification and functional characterization of a novel acetylcholine-binding protein from the marine annelid *Capitella teleta*. *Biochemistry* **49:**2279–2287.

Millar NS and Gotti C (2009) Diversity of vertebrate nicotinic acetylcholine receptors. *Neuropharmacology* **56:**237–246.

Mocharla VP, Colasson B, Lee LV, Röper S, Sharpless KB, Wong CH, and Kolb HC (2004) In situ click chemistry: enzyme-generated inhibitors of carbonic anhydrase II. *Angew Chem Int Ed Engl* **44:**116–120.

Mogg AJ, Whiteaker P, McIntosh JM, Marks M, Collins AC, and Wonnacott S (2002) Methyllycaconitine is a potent antagonist of α-conotoxin-MII-sensitive presynaptic nicotinic acetylcholine receptors in rat striatum. *J Pharmacol Exp Ther* **302:**197–204.

Mudo G, Belluardo N, and Fuxe K (2007) Nicotinic receptor agonists as neuroprotective/neurotrophic drugs: progress in molecular mechanisms. *J Neural Transm* **114:**135–147.

Nemecz A and Taylor P (2011) Creating an α7 nicotinic acetylcholine recognition domain from the acetylcholine-binding protein: crystallographic and ligand selectivity analyses. *J Biol Chem* **286:**42555–42565.

Picciotto MR and Zoli M (2008) Neuroprotection via nAChRs: the role of nAChRs in neurodegenerative disorders such as Alzheimer's and Parkinson's disease. *Front Biosci* **13:**492–504.

Purcell WP and Singer JA (1967) Electronic and molecular structure of selected unsubstituted and dimethyl amides from measurements of electric moments and nuclear magnetic resonance. *J Phys Chem* **71:**4316–4319.

Puskar NL, Xiu X, Lester HA, and Dougherty DA (2011) Two neuronal nicotinic acetylcholine receptors, $\alpha4\beta4$ and $\alpha7$, show differential agonist binding modes. *J Biol Chem* **286:**14618–14627.

Reeves PJ, Callewaert N, Contreras R, and Khorana HG (2002) Structure and function in rhodopsin: high-level expression of rhodopsin with restricted and homogeneous *N*-glycosylation by a tetracycline-inducible *N*-acetylglucosaminyltransferase I-negative HEK293S stable mammalian cell line. *Proc Natl Acad Sci USA* **99:**13419–13424.

Rostovtsev VV, Green LG, Fokin VV, and Sharpless KB (2002) A stepwise Huisgen cycloaddition process: copper(I)-catalyzed regioselective "ligation" of azides and terminal alkynes. *Angew Chem Int Ed Engl* **41:**2596–2599.

Rucktooa P, Smit AB, and Sixma TK (2009) Insight in nAChR subtype selectivity from AChBP crystal structures. *Biochem Pharmacol* **78:**777–787.

Smit AB, Syed NI, Schaap D, van Minnen J, Klumperman J, Kits KS, Lodder H, van der Schors RC, van Elk R, Sorgedrager B, et al. (2001) A glia-derived acetylcholine-binding protein that modulates synaptic transmission. *Nature* **411:**261–268.

Talley TT, Yalda S, Ho KY, Tor Y, Soti FS, Kem WR, and Taylor P (2006) Spectroscopic analysis of benzylidene anabaseine complexes with acetylcholine binding proteins as models for ligand-nicotinic receptor interactions. *Biochemistry* **45:**8894–8902.

Taly A, Corringer PJ, Guedin D, Lestage P, and Changeux JP (2009) Nicotinic receptors: allosteric transitions and therapeutic targets in the nervous system. *Nat Rev Drug Discov* **8:**733–750.

Taylor P and Insel PA (1990) Molecular basis of pharmacologic selectivity, in *Principles of Drug Action: The Basis of Pharmacology*, 3rd ed (Pratt WB and Taylor P eds) pp 1–102, Churchill Livingstone, New York.

Tornøe CW, Christensen C, and Meldal M (2002) Peptidotriazoles on solid phase: [1,2,3]-triazoles by regiospecific copper(I)-catalyzed 1,3-dipolar cycloadditions of terminal alkynes to azides. *J Org Chem* **67:**3057–3064.

Whiting M, Muldoon J, Lin YC, Silverman SM, Lindstrom W, Olson AJ, Kolb HC, Finn MG, Sharpless KB, Elder JH, et al. (2006) Inhibitors of HIV-1 protease by using in situ click chemistry. *Angew Chem Int Ed Engl* **45:**1435–1439.

Wyllie DJ and Chen PE (2007) Taking the time to study competitive antagonism. *Br J Pharmacol* **150:**541–551.

Xiu X, Puskar NL, Shanata JA, Lester HA, and Dougherty DA (2009) Nicotine binding to brain receptors requires a strong cation-pi interaction. *Nature* **458:**534–537.

Yamauchi JG, Nemecz Á, Nguyen QT, Muller A, Schroeder LF, Talley TT, Lindstrom J, Kleinfeld D, and Taylor P (2011) Characterizing ligand-gated ion channel receptors with genetically encoded Ca^{2++} sensors. *PLoS One* **6:**e16519.

Zhang L, Chen X, Xue P, Sun HH, Williams ID, Sharpless KB, Fokin VV, and Jia G (2005) Ruthenium-catalyzed cycloaddition of alkynes and organic azides. *J Am Chem Soc* **127:**15998–15999.

Address correspondence to: Palmer Taylor, Department of Pharmacology, Skaggs School of Pharmacy and Pharmaceutical Sciences, University of California, San Diego, Pharmaceutical Sciences Building, 9500 Gilman Dr., La Jolla, CA 92093-0657. E-mail: pwtaylor@ucsd.edu